The balanced act of crossmodal and intramodal plasticity for processing sound categories in early and late onset blindness

Authors:

Mattioni Stefania*[1,2], Rezk Mohamed[1], Ceren Battal[1,2], Jyothirmayi Vadlamudi [1], Collignon Olivier*[1,2]

Affiliations:

[1] Institute for research in Psychology (IPSY) & Neuroscience (IoNS), Louvain Bionics, Crossmodal Perception and Plasticity Laboratory - University of Louvain (UCLouvain), Louvain, Belgium

[2] Center for Mind/Brain Studies, University of Trento, Trento, Italy

* Correspondence should be addressed to: Stefania Mattioni (stefania.mattioni@uclouvain.be) and Olivier Collignon (olivier.collignon@uclouvain.be).

Abstract

Visual deprivation triggers enhanced dependence on auditory representation. It was suggested that (auditory) temporal regions sharpen their response to sounds in visually deprived people. In contrast with such view, we show that the coding of sound categories is enhanced in the occipital but, importantly, reduced in the temporal cortex of early and, to a lesser extent, of late blind people. Importantly, the representation of sound categories in occipital and temporal regions is characterized by a similar 'human-centric' structure in blind people, supporting the idea that these decreased intramodal and increased crossmodal representations are linked. We suggest that early, and to some extent late blindness, induces network-level reorganization of the neurobiology of sound categories by concomitantly increasing/decreasing the respective computational load of occipital/temporal regions.

Keywords: early and late blindness; auditory; multivariate analyses; fMRI; cross-modal plasticity; intra-modal plasticity.

Introduction

The occipital cortex of early blind individuals enhances its response to non-visual stimuli (Ackeren et al., 2018; Amedi, Raz, Pianka, Malach, & Zohary, 2003; Marina Bedny, Pascual-Leone, Dodell-Feder, Fedorenko, & Saxe, 2011; Collignon et al., 2011; Sadato et al., 1996). Importantly, this mechanism of crossmodal plasticity (CMP) follows organizational principles known to be routed in the occipital cortex of sighted people (Amedi, Raz, Azulay, Malach, & Zohary, 2010; Dormal & Collignon, 2011; Ricciardi, Bonino, Pellegrini, & Pietrini, 2014; Striem-Amit, Dakwar, Reich, & Amedi, 2012). For instance, we have recently shown that the Ventral Occipito-Temporal Cortex (VOTC) reliably encodes sound categories in early blind, and to a lesser extent also in sighted people, using a representational structure and connectivity partially similar to the one found in vision (Mattioni et al., 2020). However, some important questions remain unsolved.

What is the impact of visual deprivation on the brain regions coding for the remaining senses? Contradictory results emerged from previous literature about the way intra-modal plasticity expresses in early blindness. Some studies in blind humans promoted the idea that visual deprivation elicits enhanced response in the sensory cortices responsible for touch or audition (Elbert, Sterr, Rockstroh, Pantev, & Mu, 2002; Gougoux et al., 2009; Manjunath et al., 1998; Naveen et al., 1998; Pascual-leone & Torres, 1993; Rauschecker, 2002; Röder, Stock, Bien, Neville, & Rösler, 2002). In contrast to those results, several studies observed a decreased engagement of auditory or tactile sensory cortices during non-visual processing in early blind individuals (M. Bedny, Richardson, & Saxe, 2015; Burton et al., 2002; Pietrini et al., 2004; Ricciardi et al., 2009; Stevens & Weaver, 2009; Striem-Amit, Cohen, Dehaene, & Amedi, 2012; Wallmeier, Kish, Wiegrebe, & Flanagin,

2015). Those antagonist results were however both interpreted as showing improved processing in the regions supporting the remaining senses in blind people: more activity means enhanced processing and less activity means lower resources needed to achieve the same process; so both more and less means better. In this fallacious interpretational context, the application of multi-voxel pattern analysis (MVPA) methods to brain imaging data represents an opportunity to move beyond comparing mere between-groups activity level differences by allowing a detailed characterization of the information contained within brain areas (Berlot, Popp, & Diedrichsen, 2020; Kriegeskorte, Mur, & Bandettini, 2008). An intriguing possibility, is that early visual deprivation triggers a redeployment mechanism that would reallocate part of the sensory processing typically tagging the preserved senses (i.e. the temporal cortex for the auditory stimulation) to the occipital cortex deprived of its most salient visual input (Dormal, Rezk, Yakobov, Lepore, & Collignon, 2016; Hurk, Baelen, Op, & Beeck, 2017; F. Jiang, Stecker, Boynton, & Fine, 2016). A systematic investigation of information processing in both the deprived and preserved sensory cortices in the blind is, however, still missing.

A further important question that remains debated is whether and how the onset of blindness impacts on the reorganizations of the occipital regions and on their interplay with the coding of sounds implemented in temporal regions. We have recently suggested that crossmodal plasticity in early blind could be an extension of the intrinsic categorical organization of VOTC, that is partially independent from vision also in sighted (Mattioni et al., 2020; see also Amedi, Jacobson, Hendler, Malach, & Zohary, 2002; Ricciardi & Pietrini, 2011 for similar suggestions). According to this view, one should assume that crossmodal plasticity would express similarly also when the onset of blindness occurs late in life. In

contrast with this hypothesis, previous studies suggested that, despite late blind individuals showing enhanced occipital recruitment for non-visual stimuli, this recruitment might not be as functionally organized as in the case of early blindness (Marina Bedny, Pascual-Leone, Dravida, & Saxe, 2012; Collignon et al., 2013; Kanjlia, Pant, & Bedny, 2019). In addition, two studies including a small number of LB participants (n=4 in Jiang et al., 2016; n=5 LB in Stevens & Weaver, 2009) showed that the functional profile of the auditory cortex in LB might be more similar to the one of the sighted controls than to the congenitally blind group.

With those unsolved question in mind, the current study aimed to carry out a comprehensive multivariate exploration on how sound categories are encoded in the temporal and occipital cortices in decently numbered groups of early blind and late blind individuals, compared to matched sighted individuals.

Method

Participants

Fifty-two participants involved in our fMRI study: 17 early blinds (EB; 10F), 15 late blinds (LB; 4F) and 20 sighted controls (SC). We assigned the SC to 2 different groups to maximize the matching with their respective blind group: a sighted control group for the early blind (SCEB) including 17 subjects (6F) and a sighted control group for the late blind (SCLB) including 15 subjects (4F). Since some SC participants were included in both the SCEB and the SCLB groups, we never directly compared these two groups.

EB participants were congenitally blind or lost their sight very early in life and all of them reported not having visual memories and never used vision functionally (Table 1). The EB and SCEB were age (range 20-67 years, mean ± SD: 33.29 ± 10.24 for EB subjects, range 23-63 years, mean ± SD: 34.12 ± 8.69 for SCEB subjects) and gender ($X^2(33)=1.46$; $p=0.23$) matched. One EB participant was able to only perform two out of the five runs and was excluded from the analyses.

Table 1. Characteristics of early blind participants.

Subjects	Age(y)	Sex	Residual visual perception	Onset	Cause of blindness
EB1	30	M	Diffuse light	0	Damaged optic nerve
EB2	33	F	No	0	Congenital cataracts
EB3	29	F	Diffuse light	4	Retinopathy
EB4	67	M	No	0	Congenital glaucoma
EB5	39	M	Diffuse light	0	Retinopathy
EB6	26	M	No	3	Infection of the eyes
EB7	34	F	No	0	Microphtalmia
EB8	28	M	No	3	Retinopathy
EB9	29	F	Diffuse light	0	Retinopathy
EB10	43	M	No	0	Retinopathy
EB11	35	F	Diffuse light	0	Hypoxia
EB12	36	M	No	0	Hypoxia
EB13	27	F	Diffuse light	4	Retinopathy
EB14	29	F	Diffuse light	0	Retinopathy
EB15	20	F	No	0	Retinopathy
EB16	34	F	No	0	Hypoxia
EB17	27	F	No	0	Damaged optic nerve

M, male; F, female

LB participants acquired blindness late in life (range of the age of acquisition: 6-45 y.o.) and have experienced visual deprivation for 20.6 years in average (range 5-43 years). All of them reported having visual memories and having used vision functionally (table 1).

The LB and SCLB were age (range 25-68 years, mean ± SD: 44.4 ± 11.56 for LB subjects, range 30-63 years, mean ± SD: 37.7 ± 8.69 for SCLB subjects) and gender (X^2 (30)=0; p=1) matched.

All participants were blindfolded during the task. Participants received a monetary compensation for their participation. The ethical committee of the University of Trento approved this study (protocol 2014-007) and participants gave their informed consent before participation.

Materials and methods

Since this paper is submitted as a Research Advances format, it represents a substantial development that directly build upon a Research Article published previously by eLife (Mattioni et al., 2020). No extensive description of material and methods will appear when in directly overlaps with our previous publication.

Stimuli

A preliminary experiment was carried out in order to select the auditory stimuli. Ten participants who did not participate in the main experiment were presented with 4 different versions of 80 acoustic stimuli from 8 different categories (human vocalization, human non-vocalization, birds, mammals, tools, graspable objects, environmental scenes, big mechanical objects). We asked the participants to name the sound and then to rate, from 1 to 7, how representative the sound was of its category. We selected only the stimuli that were recognized with at least 80% accuracy, and among those, we choose for each category the 3 most representative sounds for a total of 24 acoustical stimuli in the final set

(see table 2). All sounds were collected from the database *Freesound* (https://freesound.org), except for the human vocalizations that were recorded in the lab. The sounds were edited and analysed using the softwares *Audacity* (http://www.audacityteam.org) and Praat (http://www.fon.hum.uva.nl/praat/). Each mono-sound (44,100 Hz sampling rate) was 2 seconds long (100msec fade in/out) and amplitude-normalized using root mean square (RMS) method.

The final acoustic stimulus set included 24 sounds from 8 different categories (human vocalization, human non-vocalization, birds, mammals, tools, graspable objects, environmental scenes, big mechanical objects) that could be reduced to 4 superordinate categories (human, animals, manipulable objects, big objects/places) (see fig. 1 and Table 2).

Table 2. Categories and stimuli.

CATEGORIES	STIMULI
BIRDS	Canary Owl Seagull
MAMMALS	Dog Donkey Horse
HUMAN VOCALIZATIONS	"*Fro*"- Woman "*BaBe*" - Man "OOO"-Man
HUMAN NON VOCALIZATIONS	Women laughing Man crying Women yawning
TOOLS	Hairdryer Saw Toothbrush
GRASPABLE OBJECTS	Guitar Keyboard Telephone
BIG MECHANICAL OBJECTS	Church-bell Traffic Train
ENVIRONMENTAL SCENES	Storm River Wind

Procedure

Before entering the scanner, all the stimuli were presented to each participant to ensure perfect recognition. In the fMRI experiment each trial consisted of the same stimulus repeated twice. Rarely (8% of the occurrences), a trial was made up of two different consecutive stimuli (catch trials). Only in this case, participants were asked to press a key with the right index finger if the second stimulus belonged to the living category and with their right middle finger if the second stimulus belonged to the non-living category. This procedure ensured that the participants attended and processed the stimuli. Each pair of

stimuli lasted 4s (2s per stimulus) and the inter-stimulus interval between one pair and the next was 2s long for a total of 6s for each trial. Within the fMRI session participants underwent 5 runs. Each run contained 3 repetitions of each of the 24 stimuli, 8 catch trials and two 20s-long periods (one in the middle and another at the end of the run). The total duration of each run was 8min and 40s. The presentation of trials was pseudo-randomized: two stimuli from the same category (i.e. animals, humans, manipulable objects, non-manipulable objects) were never presented in subsequent trials. The stimuli delivery was controlled using Matlab Psychophysics toolbox (http://psychtoolbox.org).

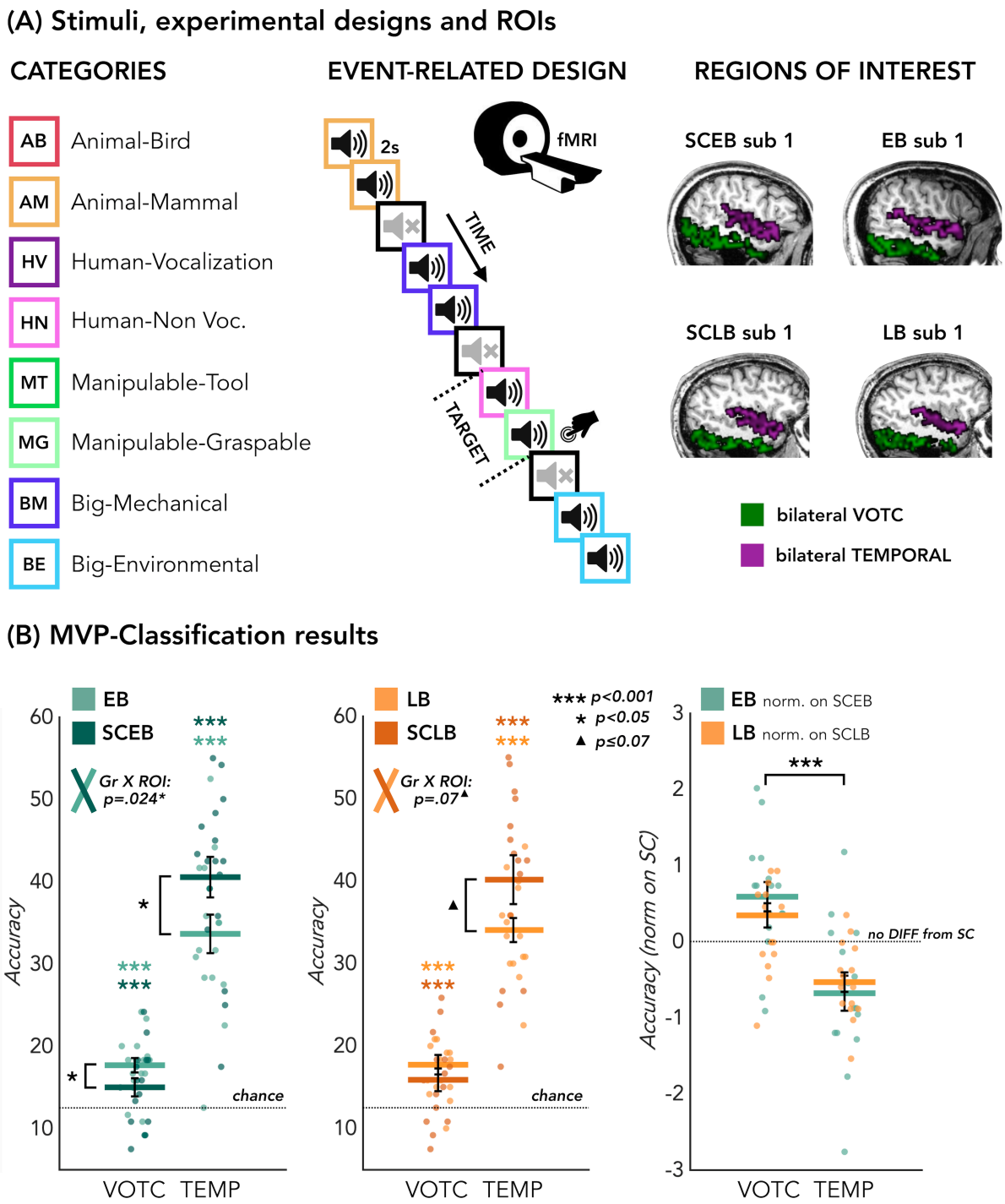

Fig. 1. Experimental design and MVP-classification results using ROIs. (A) Categories of stimuli, design of the fMRI experiment and Regions of Interest (ROIs). (B) MVP-classification results. Left panel: results from the EB/SCEB groups; central panel: results from the LB/SCLB groups; right panel: data from EB and LB are directly compared after normalizing them based on their own matched group.

fMRI data acquisition and analyses

fMRI data acquisition and preprocessing

We acquired our data on a 4T Bruker Biospin MedSpec equipped with an eight-channel birdcage head coil. Functional images were acquired with a T2*-weighted gradient-recalled echo-planar imaging (EPI) sequence (TR, 2000 ms; TE, 28 ms; flip angle, 73°; resolution, 3x3 mm; 30 transverses slices in interleaved ascending order; 3mm slice thickness; field of view (FoV) 192x192 mm2). The four initial scans were discarded to allow for steady-state magnetization. Before each EPI run, we performed an additional scan to measure the point-spread function (PSF) of the acquired sequence, including fat saturation, which served for distortion correction that is expected with high-field imaging.

A structural T1-weighted 3D magnetization prepared rapid gradient echo sequence was also acquired for each subject (MP-RAGE; voxel size 1x1x1 mm; GRAPPA acquisition with an acceleration factor of 2; TR 2700 ms; TE 4,18 ms; TI (inversion time) 1020 ms; FoV 256; 176 slices).

To correct for distortions in geometry and intensity in the EPI images, we applied distortion correction on the basis of the PSF data acquired before the EPI scans (Zeng & Constable, 2002). Raw functional images were pre-processed and analysed with SPM8 (Welcome Trust Centre for Neuroimaging London, UK; http://www.fil.ion.ucl.ac.uk/spm/software/spm/) implemented in MATLAB (MathWorks). Pre-processing included slice-timing correction using the middle slice as reference, the application of temporally high-pass filtered at 128 Hz and motion correction.

Regions of interest

The anatomical scan was used to reconstruct the cortical surface of each hemisphere using FreeSurfer (http://surfer.nmr.mgh.harvard.edu). The cortical anatomic segmentation was performed according to the Desikan-Killiany atlas (Desikan et al., 2006).

Six ROIs were then selected in each hemisphere: Lateral Occipital, Fusiform, Parahippocampal and Infero-Temporal areas for the visual ROIs and the Transverse Temporal and the Superior Temporal areas for the acoustic ROIs. Then, we combined these areas in order to obtain one bilateral ventral occipital-temporal (VOTC) ROI and one bilateral temporal ROI (figure 1). We focused on those regions known to be involved in categorical representation, for this reason we did not include primary auditory and visual cortices. Our strategy to work on a limited number of relatively large brain parcels has the advantage to minimize unstable decoding results collected from small regions (Norman, Polyn, Detre, & Haxby, 2006) and reduce multiple comparison problems intrinsic to neuroimaging studies (Etzel, Zacks, & Braver, 2013). All further analyses were carried out in subject space for enhanced anatomical precision and to avoid spatial normalization across subjects.

General linear model

The pre-processed images for each participant were analyzed using a general linear model (GLM). For each of the 5 runs we included 32 regressors: 24 regressors of interest (each stimulus), 1 regressor of no-interest for the target stimuli to be detected, 6 head-motion regressors of no-interest and 1 constant. From the GLM analysis we obtained a β-image for each stimulus (i.e. 24 sounds) in each run, for a total of 120 (24 x 5) beta maps.

Topographical selectivity map

For this analysis, we needed all participants to be coregistered and normalized in a common volumetric space. To achieve maximal accuracy, we relied on the DARTEL (Diffeomorphic Anatomical Registration Through Exponentiated Lie Algebra (Ashburner, 2007) toolbox. DARTEL normalization takes the grey and white matter templates from each subject to create an averaged template based on our own sample that will be used for the normalization. The creation of a study-specific template using DARTEL was performed to reduce deformation errors that are more likely to arise when registering single subject images to an unusually shaped template (Ashburner, 2007). This is particularly relevant when comparing blind and sighted subjects given that blindness is associated with significant changes in the structure of the brain itself, particularly within the occipital cortex (Dormal et al., 2016; J. Jiang et al., 2009; Pan et al., 2007; Park et al., 2009).

We created a topographical selectivity map for each ROI (VOTC and TEMP) and for each group. Only for this analysis, we included also the maps form an additional group of sighted that performed a visual version (SCv) of the same experiment (for further details see Mattioni et al., 2020).

To create the topographical selectivity map (Fig. 2) we extracted in each participant the β-value for each of our 4 main conditions (animals, humans, manipulable objects and places) from each voxel inside each mask and we assigned to each voxel the condition producing the highest β-value (winner takes all). This analysis resulted in specific clusters of voxels that spatially distinguish themselves from their surround in terms of selectivity for a particular condition (Hurk et al., 2017, Mattioni et al., 2020).

Finally, to compare how similar are the topographical selectivity maps in the 3 groups we followed, for each pair of groups [i.e. 1) SCv-EB; 2) SCv-SCEB; 3) SCv-LB; 4) SCv-

SCLB; 5) SCEB-EB; 6) SCLB-LB; 7) EB-LB] these steps: (1) We computed the Spearman's correlation between the topographical selectivity map of each subject from Group 1 with the averaged selectivity map of Group 2 and we computed the mean of these values. (2) We computed the Spearman's correlation between the topographical selectivity map of each subject from Group 2 with the averaged selectivity map of Group 1 and we computed the mean of these values. (3) We averaged the 2 mean values obtained from step 1 and step 2, in order to have one mean value for each group comparison.

To test statistical differences we used a permutation test (10.000 iterations): (4) We randomly permuted the conditions of the vector of each subject from Group 1 and of the mean vector of Group 2 and we computed the correlation (as in Step 1). (5) We randomly permuted the conditions of the vector of each subject from Group 2 and of the mean vector of Group 1 and we computed the correlation (as in Step 2). Importantly, we constrained the permutation performed in the step 4 and 5 in order to take into consideration the inherent smoothness/spatial dependencies in the univariate fMRI data. In each subject, we individuated each cluster of voxels showing selectivity for the same category and we kept these clusters fixed in the permutation, assigning randomly a condition to each of these predefined clusters. In this way, the spatial structure of the topographical maps was kept identical to the original one, making very unlikely that a significant result could be explained by the voxels' spatial dependencies. We may however note that this null-distribution is likely overly conservative since it assumes that size and position of clusters could be created only from task-independent spatial dependencies (either intrinsic to the acquisition or due to smoothing). We checked that each subject has at least 7 clusters in his topographical map, which is the minimal number to reach the

10000 combinations needed for the permutation given our four categories tested (possible combinations= $n_categories^{n_clusters}$; 4^7=16384). (6) We averaged the 2 mean values obtained from step 4 and step 5. (7) We repeated these steps 10.000 times to obtain a distribution of correlations simulating the null hypothesis that the two vectors are unrelated (Kriegeskorte et al., 2008). If the actual correlation falls within the top **α** × 100% of the simulated null distribution of correlations, the null hypothesis of unrelated vectors can be rejected with a false-positives rate of **α**. For each ROI the p values are reported after FDR correction (for 7 comparisons).

To test the difference between the group pairs' correlations (we only test if in VOTC the correlation between the topographical maps of SCv and EBa was different from the correlation of SCv and SCEB and if the correlation between SCv and LB was different from the correlation of SCv and SCLB) we used a permutation test (10.000 iterations): (8) We computed the difference between the correlation of Pair 1 and Pair 2: mean correlation Pair1 – mean correlation Pair2. (9) We kept fixed the labels of the group common to the 2 pairs and we shuffled the labels of the subjects from the other two groups (e.g. if we are comparing SCv-EB versus SCv-SCEB, we keep the SCv group fixed and we shuffle the labels of EB and SCEB). (10) After shuffling the groups' labels we computed again the point 1-2-3 and 8. (11) We repeated this step 10.000 times to obtain a distribution of differences simulating the null hypothesis that there is no difference between the two pairs' correlations. If the actual difference falls within the top **α** × 100% of the simulated null distribution of difference, the null hypothesis of absence of difference can be rejected with a false-positives rate of **α**.

Multivoxel pattern (MVP) classification

MVP classification analysis was performed using the CoSMoMVPA (Oosterhof, Connolly, & Haxby, 2016) toolbox, implemented in Matlab (Mathworks). We tested the discriminability of patterns for the eight categories using linear discriminant analysis (LDA). We performed a leave-one-run-out cross-validation procedure using beta-estimates from 4 runs in the training set, and the beta-estimates from the remaining independent run to test the classifier, with iterations across all possible training and test sets. This procedure was implemented in both ROIs: we first extracted the 250 most discriminative voxels according to our 8 categories (De Martino et al., 2008; Mitchell & Wang, 2007) and we ran MVP classification on this subset of voxels using the parameters described above.

Statistical significance of the classification results within each group was assessed using a non-parametric technique by combining permutations and bootstrapping (Stelzer, Chen, & Turner, 2013). For each subject, the labels of the different categories' conditions were permuted, and the same decoding analysis was performed. The previous step was repeated 100 times for each subject. A bootstrap procedure was applied in order to obtain a group-level null distribution that is representative of the whole group. From each subject's null distribution, one value was randomly chosen (with replacement) and averaged across all participants. This step was repeated 100,000 times resulting in a group level null distribution of 100,000 values. The statistical significance of our MVP classification results was estimated by comparing the observed result to the group-level null distribution. This was done by calculating the proportion of observations in the null distribution that had a classification accuracy higher than the one obtained in the real test. To account for the multiple comparisons, all p-values were corrected using false discovery rate (FDR) (Benjamini & Hochberg, 1995).

The statistical difference between each group of blind (EB and LB) and their own sighted control group (SCEB and SCLB) was assessed using a permutation test. We built a null distribution for the difference of the accuracy values of the two groups by computing them after randomly shuffling the group labels. We repeated this step 10000 times. The statistical significance was estimated by comparing the observed result (i.e. the real difference of the accuracy between the two groups) to the null distribution. This was done by calculating the proportion of observations in the null distribution that had a difference of classification accuracy higher than the one obtained in the real test. To account for the multiple comparisons, all p-values were corrected using false discovery rate (FDR) (Benjamini and Hochberg, 1995).

To analyze the interaction between groups and regions, we also performed a non-parametric test: the adjusted ranked transform test (ART) (Leys &Schumann, 2010). ART is an advisable alternative to a factorial ANOVA when the requirements of a normal distribution and of homogeneity of variances are not fulfilled (Leys & Schumann, 2010), which is often the case of multivariate fMRI data (Stelzer et al., 2013). Importantly, we used the adjusted version of the original rank transformation (RT) test (Conover & Iman, 1981). In fact, the classical RT method loses much of its robustness as soon as the main effects occur together with one or several interactions. To avoid this problem, in the adjusted version the scores are adjusted by deducting the main effects and then analyzing separately the interactions (Leys & Schumann, 2010).

We performed two ART tests, one for each blind group and its own sighted control group. The first ART with Lobe (occipital and temporal) as within-subject factor and with

SCEB and EB Groups as between-subjects factor. The second ART with Lobe (occipital and temporal) as within-subject factor and with SCLB and LB Groups as between-subjects factor.

Early and the late blind groups were not matched for age and gender due to the difficulty of recruit a sufficient number of blind participants using stringent inclusion criteria. To be able to compare both groups, we applied a normalization of the data from each blind group based on its own sighted control group. Then, we directly tested the statistical difference between the normalized data of EB and LB using the same statistical procedure as described above.

Representational similarity analysis (RSA)

We further investigated the functional profile of the ROIs using RSA. This analysis can do a step further compared to the decoding analysis, revealing the way used by each region to represent the different categories. In fact, a similar level of decoding could be driven by different ways the categories are represented across groups or brain regions. RSA is a well-suited tool to break this code and to deepen the way brain regions represent our stimuli. RSA analysis is based on the concept of dissimilarity matrix (DSM): a square matrix where the columns and rows correspond to the number of the conditions (8X8 in this experiment) and it is symmetrical about a diagonal of zeros. Each cell contains the dissimilarity index between two stimuli (Kriegeskorte & Kievit, 2013). This abstraction from the activity patterns themselves represents the main strength of RSA, allowing a direct comparison of the information carried by the representations in different brain regions, different groups and even between brain and models (Kriegeskorte & Mur, 2012; Kriegeskorte, Mur, & Bandettini, 2008).

First, we computed the brain dissimilarity matrices for each ROI and in each subject. We extracted the DSM (Kriegeskorte, Mur, Ruff, et al., 2008) in each ROI, computing the dissimilarity between the spatial patterns of activity for each pair of conditions. To do so, we first extracted in each participant and in every ROI the stimulus-specific BOLD estimates from the contrast images for all the 8 conditions separately. Then, we used the linear discriminant contrast (LDC) to compute the distance between each pair of patterns. The LDC distance is a cross-validated estimate of the Malhanobis distance (also known as crossnobis distance). The cross-validation across runs avoids that the run-specific noise systematically affects the estimated distances between neural patterns, which makes possible to test the distances directly against zero. Therefore, the LDC distance provides a measurement on a ratio scale with an interpretable zero value that indicates an absence of distance between conditions (Evans, Price, Diedrichsen, Gutierrez-Sigut, & MacSweeney, 2019; Walther et al., 2016).

Importantly, since the DSMs are symmetrical matrices, for all the RSA analyses we always use the upper triangular DSM (excluding the diagonal).

We used these brain DSMs for several analyses: (1) Correlation between VOTC and Temporal ROIs in each subject and group; (2) Hierarchical clustering analysis on the averaged DSMs' correlation across groups and ROIs; (3) Comparison between brain DSMs and different representational models based on our stimuli space. The rational and detailed description of each analysis is reported below.

RSA - Correlation between VOTC and Temporal ROIs in each subject and group.

When the sound of our 8 categories are presented, brain regions create a representation of these sounds, considering some categories more similar and others more

different. How similar are the representations embedded in the temporal cortex and in VOTC? Would visual deprivation have an impact on the structure of representation for sound categories in VOTC? Our hypothesis was that the similarity between the representation of the 8 sound categories between temporal and occipital regions was enhanced in blind individuals compared to their sighted controls. To test this hypothesis, we compared the correlation between the DSMs of VOTC and temporal ROIs in each group.

In each individual we computed the Spearman's correlation between the VOTC and temporal DSMs. We then averaged the values across subjects from the same group to have a mean value per group (Fig 2A).

For statistical analysis we followed the procedure suggested by Kriegeskorte and collaborators (2008). For each group, the statistical difference from zero was determined using permutation test (10000 iterations), building a null distribution for these correlation values by computing them after randomly shuffling the labels of the matrices. Similarly, the statistical difference between groups was assessed using permutation test (10000 iterations) building a null distribution for these correlation values by computing them after randomly shuffling the group labels. The p-values are reported after false discovery rate (FDR) correction implemented using the Matlab function 'mafdr'.

Finally, to directly compare the correlation from the early and the late blind subjects, which are not matched for age and gender, we applied a normalization of the data from each blind group based on its own sighted control group. Then, we tested the statistical difference between the normalized data of EB and LB using the same non-parametric statistical procedure described above.

RSA - Hierarchical clustering analysis based on DSM's correlation across subjects and ROIs

Some important information could also arise looking at the similarities of the categorical representations across groups and regions. Since we are looking at the activity for auditory stimulation in the "visual" cortex, it is interesting to understand if the representational structure of VOTC in blind individuals does remodel itself to be closer to the one of their temporal cortex or if it, anyway, keeps a shape similar to the one of VOTC in sighted for sounds. In other words, would the representation of VOTC in EB be closer to the representation of VOTC in SCEB or to the representation of the temporal parcels (both in EB and in SCEB)? And what about the representation of VOTC in LB?

Figure 3B represents all the possible comparisons of regions and groups that we can investigate. Importantly, applying a hierarchical clustering approach on these data (King et al., 2019), we can go beyond the correlation values and look at how these DSMs would cluster according to their (dis)similarity.

For both pairs of groups (EB-SCEB and LB-SCLB) there are 6 possible combinations to compare (see fig. 3B). For instance, in the EB-SCEB case the combinations are: (1) VOTC-EB/TEMP-EB; (2) VOTC-SCEB/TEMP-SCEB; (3) VOTC-EB/VOTC-SCEB; (4) TEMP-EB/TEMP-SCEB; (5) VOTC-EB/TEMP-SCEB; (6) VOTC-SCEB/TEMP-EB. First, we compared the representation of the categories between each of these combinations of group/region (see supplemental material for details on the procedure and the statistical analyses).

Then, we implemented a hierarchical clustering approach (King et al., 2019) on these data, to better understand the structure of similarity between the brain regions and groups. For each pair of groups separately (EB-SCEB and LB-SCLB), we built a second order

DSM in which each row and column represent one DSM of a specific group (e.g. VOTC of EB). This resulted in a 4X4 matrix in which each line and each row represents one ROI per group (i.e. for the early blind & their control group: VOTC-EB; VOTC-SCEB; TEMP-EB; TEMP-SCEB; for the late blind & their control group: VOTC-LB; VOTC-SCLB; TEMP-LB; TEMP-SCLB).

First, we created a hierarchical cluster tree for both DSMs using the 'linkage' function in Matlab, then we defined clusters from this hierarchical cluster tree with the 'cluster' function in Matlab. Hierarchical clustering starts by treating each observation as a separate cluster. Then, it identifies the two clusters that are closest together, and merges these two most similar clusters. This continues until all the clusters are merged together or until the clustering is 'stopped' to a n number of clusters. We stopped the clustering at n=2 clusters, based on the fact that we have 2 ROIs.

RSA - Comparison between brain DSMs and representational models based on our stimuli space.

Based on which dimensions are the 8 sound categories represented in the temporal and in the occipital parcels in our groups? To address this question, we compared the representation of the sound categories in the two ROIs in each group with different representational models based either on low-level acoustic properties of the sounds or on different kind of categorical/high-level representations. Which of these models would better describe the representation of the sound stimuli in each region and group? Would the winning model (i.e. the model eliciting the highest correlation) be the same in VOTC and in the temporal region in (early and late) blind and in sighted subjects?

First of all, we built several representational models (see fig. 4-supplemental fig.2) based on different categorical ways of clustering the stimuli or on specific acoustic features of the sounds (computed using Praat, https://praat.en.softonic.com/mac).

Three models are based on low level properties of the sounds (models from 1 to 3) and 7 models are based on high level properties of the stimuli (models from 4 to 10), for a total of 10 representational models (See figure 4 – supplemental fig2 to visualize the complete set of models and the correlation between them):

1. Harmonicity-to-noise (HNR) ratio model. The HNR represents the degree of acoustic periodicity of a sound.
2. Pitch model. The pitch, calculated with the autocorrelation method (Mattioni et al. 2020), represents the measure of temporal regularity of the sound and corresponds to the perceived frequency content of the stimulus.
3. Spectral centroid model. The spectral center of gravity is a measure for how high the frequencies in a spectrum are on average.
4. Animate-inanimate model which assumes that all the animate categories cluster together and all the inanimate categories cluster together.
5. Four categories model: it assumes that the categories gather together into 4 distinct clusters representing the 4 main categories (i.e. (1) animals, (2) humans, (3) manipulable objects, (4) big object & places).
6. Behavioral model: based on the subject's ratings of similarity. We included one behavioral model for each group.
7. Human model: it assumes that the human categories cluster together vs all other categories that create a second cluster.

8. Animal model: it assumes that the animal categories cluster together vs all other categories that create a second cluster.
9. Manipulable model: it assumes that the manipulable object categories cluster together vs all other categories that create a second cluster.
10. Big & Place model: it assumes that the Big object & Place categories cluster together vs all other categories that create a second cluster.

Then, we computed the Spearman's correlation between each model and the DSM of each subject from VOTC and from the TEMP ROI. For each region separately, we finally averaged the correlation values of all subjects from the same group.

For each group, we computed the statistical difference from zero following the procedure suggested by Kriegeskorte and collaborators (2008). A permutation test (10000 iterations) was implemented to build a null distribution for these correlation values by computing them after randomly shuffling the labels of the matrices. The statistical significance, for each model, was estimated by comparing the observed result (i.e. the real correlation) to the null distribution. This was done by calculating the proportion of observations in the null distribution that had a correlation value higher than the one obtained in the real test. To account for the multiple comparisons, all p-values were corrected using false discovery rate (FDR) correction across the 10 comparisons for each ROI (Benjamini and Hochberg, 1995). We also compared the correlations across all pairs of models within each ROI, in order to test which model was the best predictor of the variance in brain RDMs in each ROI. For these pairwise comparisons, we implemented a two-sided Wilcoxon signed-rank tests and only significant (i.e. $p \leq 0.05$) FDR corrected values (for 55 comparisons) are reported in fig. 4 (Tsantani, Storrs, & Williams, 2020).

To partially foreshadow the results, this analysis revealed that the human model is the winner model in the temporal parcel of each group and that it is the winner model in VOTC of blind subjects (both EB and LB) but not of sighted.

Therefore, only for the human model we perform some statistical analyses to look at the comparison between groups (EB vs SCEB & LB vs SCLB) in both temporal and occipital ROIs. (fig 4- supplemental fig.1)

The statistical difference between each group of blind (EB and LB) and their own sighted control group (SCEB and SCLB) was assessed using a permutation test. We built a null distribution for the difference of the correlation values of the two groups by computing them after randomly shuffling the group labels. We repeated this step 10000 times. The statistical significance was estimated by comparing the observed result (i.e. the real difference of the correlations between the two groups) to the null distribution. This was done by calculating the proportion of observations in the null distribution that had a difference of correlation higher than the one obtained in the real test. To account for the multiple comparisons, all p-values were corrected using false discovery rate (FDR) (Benjamini and Hochberg, 1995).

Similarly to the MVP- classification analysis, we performed the non-parametric adjusted ranked transform test (ART) to analyze the interaction between groups and regions (Leys &Schumann, 2010).

Finally, we wanted to directly compare the correlation from the early and the late blind subjects, which are not matched for age and gender. To be able to compare these data, we applied a normalization of the data from each blind group based on its own

sighted control group. Then, we directly tested the statistical difference between the normalized data of EB and LB using the same statistical procedure described above.

Results

Topographical selectivity map

Fig. 2 represents the topographical selectivity maps, which show the voxel-wise preferred stimulus condition based on a winner take-all approach (for the four main categories: animals, humans, small objects & places) in VOTC (fig. 2A) and in the temporal ROI (fig. 2B).

In VOTC we found that the topographical auditory selectivity maps of the early blind subjects partially matched the visual map obtained in sighted controls during vision (r=0.18, p=0.0001). In addition, a similar selectivity map was also observed in the SCEB using sounds (r=0.07, p=0.0002). These results replicate our previous results in Mattioni et al., 2020. Importantly for the goal of the present experiment, we found similar results also in the LB group. The auditory selectivity maps of the late blind subjects partially matched the visual map obtained in sighted controls during vision (r=0.16, p=0.0001). In addition, a similar selectivity map was also observed in the SCLB using sounds (r=.08, p=0.0001). Finally, the correlation between the topographic maps of EB and LB was significant (r=0.12, p=0.0001).

The magnitude of the correlation between EB and SCv topographical category selective maps was significantly increased when compared to the correlation between SCEB and SCv (p=0.03). We found a similar trend also in the case of late blind: the magnitude of

correlation between LB and SCv was higher than the correlation between SCLB and SCv (p=0.08).

In the temporal ROI we found that the auditory selectivity maps were significantly similar between each group: EB-SCEB(r=.17, p=0.0002), LB-SCEB (r=.18, p=0.0002), EB-LB (r=.17, p=0.0002). However, the correlation of the visual selectivity map was not significantly correlated with none of the auditory map (SCv-EB: r=–.03,p=0.99; SCv-SCEB: r=–.02,p=0.99; SCv-LB: r=,–.05 p=0.99; SCv-SCLB: r=–.02, p=0.99).

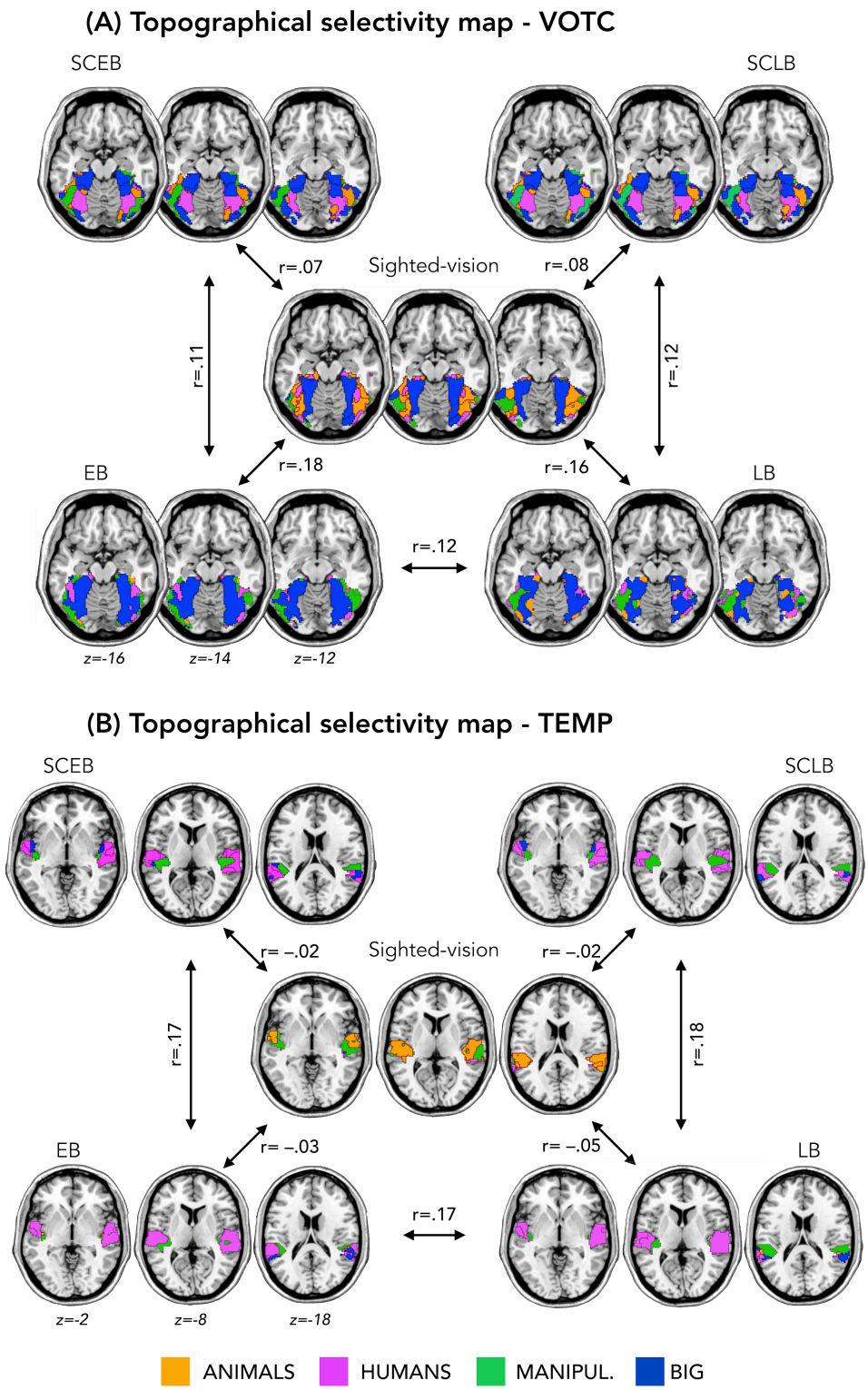

Fig. 2. Topographical selectivity maps. Averaged untresholded topographical selectivity maps for the early blind (EB, bottom left), and their matched sighted controls (SCEB, top left), the late blind (LB, bottom right) and their matched sighted controls (SCLB, top left). In the center we also reported the map from an additional group of sighted that perform the visual version of the experiment. These maps visualize the functional topography of VOTC and TEMP to the main four categories in each group. These group maps are created for visualization purpose only since statistics are run from single

subject maps (see methods). To obtain those group maps, we first averaged the β-values among participants of the same group in each voxel inside the VOTC and inside the TEMP mask for each of our 4 main conditions (animals, humans, manipulable objects and places) separately and we then assigned to each voxel the condition producing the highest β-value.

Multivoxel pattern (MVP) classification

MVPA results for the EB / SCEB groups are represented in figure 1B (left panel). In the SCEB group the decoding accuracy (DA) of the 8 categories is significantly different from chance level (12.5%) in both VOTC (DA= 15%; $p<0.001$) and temporal (DA=38%; $p<0.001$) ROIs. In the EB group the decoding accuracy of the 8 categories is also significant in the 2 ROIs: VOTC (DA=18%; $p<0.001$) and temporal (DA=33%; $p<0.001$). Importantly for our study, a permutation test also revealed a significant difference between groups in both regions. In VOTC the accuracy values are significantly higher in EB compared than the SCEB (p=0.03), while in the temporal ROI the accuracy values are significantly higher in SCEB than EB (p=0.03).

Finally, the adjusted rank transform test (ART) 2 Groups X 2 ROIs revealed a significant effect of interaction group by region ($F_{(1,31)}=5.647$; p=0.024).

MVPA results for the LB / SCLB groups are represented in figure 1B (central panel). In the SCLB group the decoding accuracy is significant in both VOTC (DA= 16%; $p<0.001$) and temporal (DA=39%; $p<0.001$). In the LB group the decoding accuracy is also significant in the 2 ROIs: VOTC (DA=18%; $p<0.001$) and temporal (DA=33%; $p<0.001$). The permutation test did not reveal a significant difference between groups in the VOTC (p=0.15), while in the temporal ROI it revealed a tendency for a decreased accuracy value in the LB compared to SCLB (p=0.07).

The ART test 2 Groups X 2 ROIs revealed a marginally significant effect of interaction group by region ($F_{(1,28)}$=3.5076; p=0.071).

Finally, we directly compared the accuracies from the early and the late blind subjects, after a normalization of the data from each blind group based on its own sighted control group (Fig 1B, right panel). The permutation test did not reveal any difference between the two groups neither in VOTC (p=0.12) nor in the temporal ROI (p=0.3).

The ART test (2 Groups X 2 ROIs) did not reveal any significant effect of interaction group by region ($F_{(1,28)}$=2.91; p=0.1).

Representational similarity analysis (RSA)

Correlation between Occipital and Temporal ROIs in each subject and group

The results for this analysis are represented in figure 3A. We look at whether the representation of the 8 sound categories shares any similarity between the VOTC and the temporal parcels within each blind and sighted subject, with particular interest at group differences. The permutation test revealed a significant correlation between the functional profile of VOTC and the functional profile of the temporal region in all groups (p<0.001 for all groups). When we look at the differences between groups, we found a significant difference between the EB and the SCEB groups (p=0.04, FDR corrected), highlighting an increased similarity between the VOTC and the temporal DSMs in the EB when compared to the SCEB group (Fig 3A – left panel). The difference between the LB and the SCLB (Fig 3A – central panel) was not significantly different (p=0.10). We also directly compared the EB and LB groups after normalizing the data based on their own sighted control groups (Fig. 3A – right panel). The permutation test did not reveal a significant difference between the two groups of blind subjects (p=0.21).

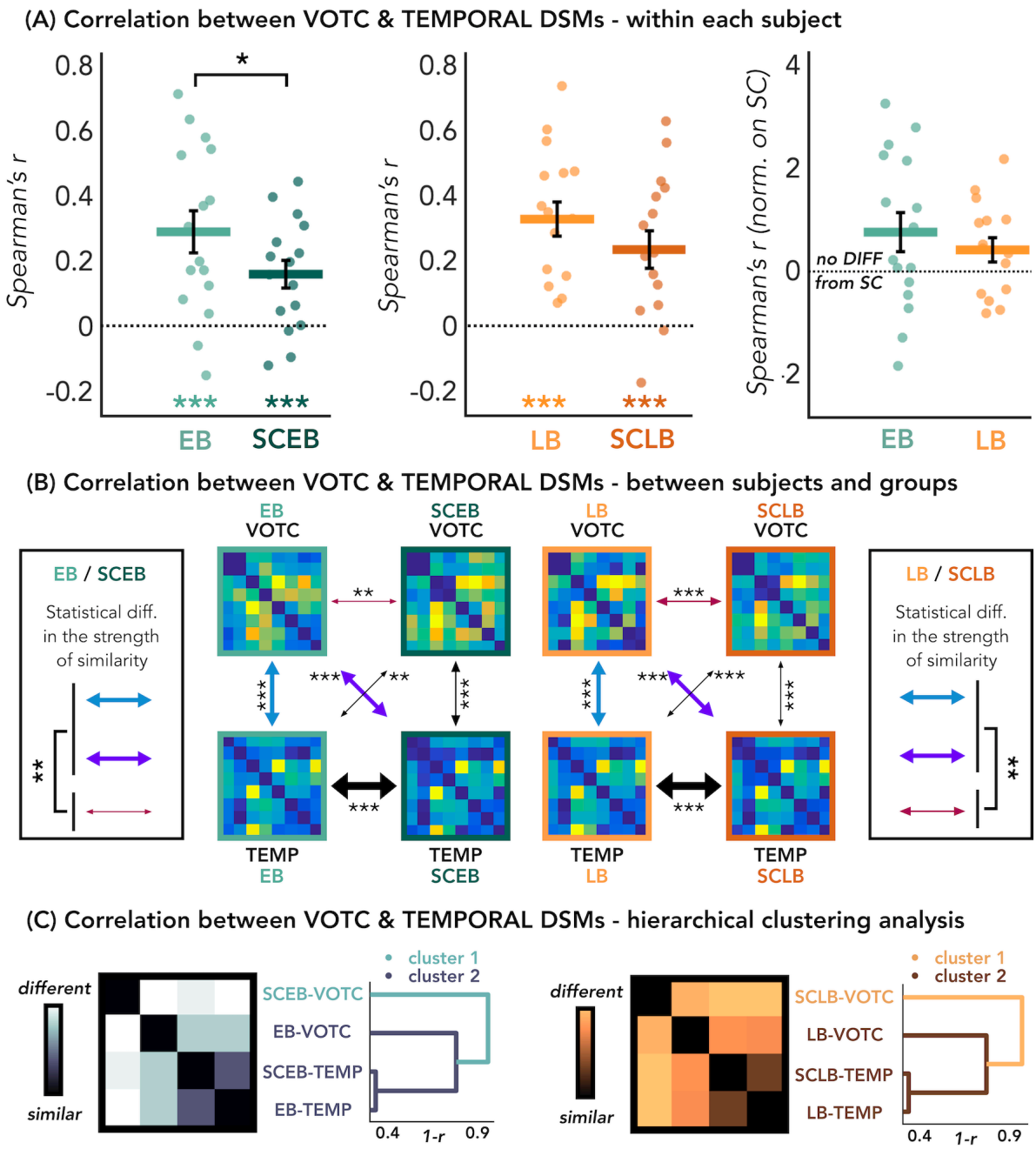

Fig. 3. Correlation between VOTC and TEMP DSMs. (A) Correlation between VOTC and TEMPORAL DSMs within each subjects. Each dot represents the Spearman's correlation of each subject between its own VOTC and TEMP DSMs. Left panel: results from the EB/SCEB groups; central panel: results from the LB/SCLB groups; right panel: data from EB and LB are directly compared after normalizing them based on their own matched group. (B) Correlation between VOTC and TEMPORAL DSMs between subjects and groups. Each matrix represents the group averaged DSM of each ROI (top row: VOTC, bottom row: TEMP). The arrows between each pair of matrices represents the averaged Spearman's correlation between the 2 DSMs. Thicker the arrow, higher the correlation value. In the box on the left side (EB/SCEB) and on the right side (LB/SCLB) we report the statistical differences in the strength of similarity between the most important pair of matrices (color-coded in red, light-blue and purple).

RSA - Hierarchical clustering analysis based on DSM's correlation across subjects and ROIs

We run this analysis to look at the similarities of the categorical representations across groups and regions. Fig. 3B represents the correlation results between all the DSMs (see the arrows between each pair of DSMs): the thicker the arrow, the higher the correlation.

In the EB-SCEB data (Fig 3B – left panel), the permutation analysis revealed that the correlation values between each possible combination were all significantly different than zero. Correlation values and related p values are reported in Table 3.

DSMs	TEMP EB	VOTC SCEB	TEMP SCEB
VOTC EB	r=.3; p=0.004	r=.09; p=0.004	r=.28; p<0.001
TEMP EB	--	r=.09; p<0.001	r=.67; p<0.001
VOTC SCEB	--	--	r=.13; p<0.001

Table 3. P values resulting from the permutation test on the correlation between DSMs' pairs. The p values are FDR corrected for 6 comparisons.

We also tested the statistical difference in the strength of the correlations (i.e. the difference between the thickness of the arrows). In figure 3B, in the lateral boxes, we only reported the statistical results for the comparisons that were more important for the aim of this study. We found that the strength of the correlation between the VOTC DSM in EB and the VOTC DSM in SCEB (red arrow in figure 3B,left panel) is significantly lower compared to the strength of correlation between the VOTC DSM in EB and the TEMP DSM in EB (light blue arrow in figure 3B, left panel) and also compared to the strength of correlation between the VOTC DSM in EB and the TEMP DSM in SCEB (purple arrow in figure 3B, left panel). The totality of the correlation values and related p values is reported in Table 4.

DSMs pairs	VOTC SCEB-TEMP SCEB	VOTC EB-TEMP SCEB	TEMP EB-VOTC SCEB	VOTC EB-VOTC SCEB	TEMP EB-TEMP SCEB
VOTC EB-TEMP EB	p=0.002	n.s.	p<0.001	p=0.001	p<0.001

VOTC SCEB-TEMP SCEB	--	p=0.002	n.s.	n.s.	p<0.001
VOTC EB-TEMP SCEB	--	--	p<0.001	p=0.001	p<0.001
TEMP EB-VOTC SCEB	--	--	--	n.s.	p<0.001
VOTC EB-VOTC SCEB	--	--	--	--	p<0.001

Table 4. P values resulting from the permutation test on the strength's difference of the correlation between DSMs. The p values are FDR corrected for 15 comparisons.

Very similar results emerged for the LB-SCLB groups (figure 3B, right panel).

The permutation analysis revealed that the correlation values between each possible combination were all significantly different than zero. Correlation values and related p values are reported in table 5.

DSMs	TEMP LB	VOTC SCLB	TEMP SCLB
VOTC LB	r=.38; p<0.001	r=.24; p<0.001	r=.34; p<0.001
TEMP LB	--	r=.17; p<0.001	r=.65; p<0.001
VOTC SCLB	--	--	r=.16; p<0.001

Table 5. P values resulting from the permutation test on the correlation between DSMs' pairs. The p values are FDR corrected for 6 comparisons.

We also tested the statistical difference in the strength of the correlations (i.e. the difference between the thickness of the arrows). In figure 3B, in the lateral boxes, we only reported the statistical results for the comparisons that were more important for the aim of this study. We found that the strength of the correlation between the VOTC DSM in LB and the VOTC DSM in SCLB (red arrow in figure 3B,right panel) is significantly lower compared to the strength of correlation between the VOTC DSM in LB and the TEMP DSM in LB (light blue arrow in figure 3B, right panel) and also compared to the strength of correlation between the VOTC DSM in LB and the TEMP DSM in SCLB (purple arrow in figure 3B, right panel). The totality of the correlation values and related p values is reported in Table 6.

DSMs pairs	VOTC SCLB-TEMP SCLB	VOTC LB-TEMP SCLB	TEMP LB-VOTC SCLB	VOTC LB-VOTC SCLB	TEMP LB-TEMP SCLB
VOTC LB-TEMP LB	p<0.001	n.s.	p<0.001	p=0.01	p<0.001
VOTC SCLB-TEMP SCLB	--	p<0.001	n.s.	n.s.	p<0.001
VOTC LB-TEMP SCLB	--	--	p=0.0015	p=0.01	p<0.001
TEMP LB-VOTC SCLB	--	--	--	n.s.	p<0.001

VOTC LB-VOTC SCLB	--	--	--	--	p<0.001

Table 6. P values resulting from the permutation test on the strength's difference of the correlation between DSMs. The p values are FDR corrected for 15 comparisons.

Crucially, we applied a hierarchical clustering analysis to these correlation values, in order to explore our data beyond the correlation. How would cluster the DSMs from each group and region based on the degree of their (dis)similarity? Fig. 2C depicts the dissimilarity matrices representing the correlation between the functional profile of each ROI and group, for EB-SCEB and for LB-SCLB separately.

On the right side of the DSM, we report the result from the hierarchical clustering analysis: in the dendrogram plots you can observe that 2 color-coded clusters emerged from this analysis. In the case of EB-SCEB data, we found that the functional profile of VOTC of EB is grouping together with the functional profile of the temporal regions both of EB and SCEB, while the VOTC of SCEB creates an isolated cluster. The same profile emerged also for the LB-SCLB data, in which the functional profile of VOTC of LB merges together with the functional profile of the temporal regions of both LB and SCLB, while the VOTC of SCLB creates an isolated cluster.

Comparison between brain DSMs and different representational models based on our stimuli space.

What could explain the clustering of the DSMs? Is there a specific feature that makes the structure of the VOTC DSM of blind closer to the TEMP DSMs? The RSA comparisons with representational models gave us some hints about what could be one of the main factors driving the observed clustering results.

Results from the correlation with representational models are represented in fig. 4.

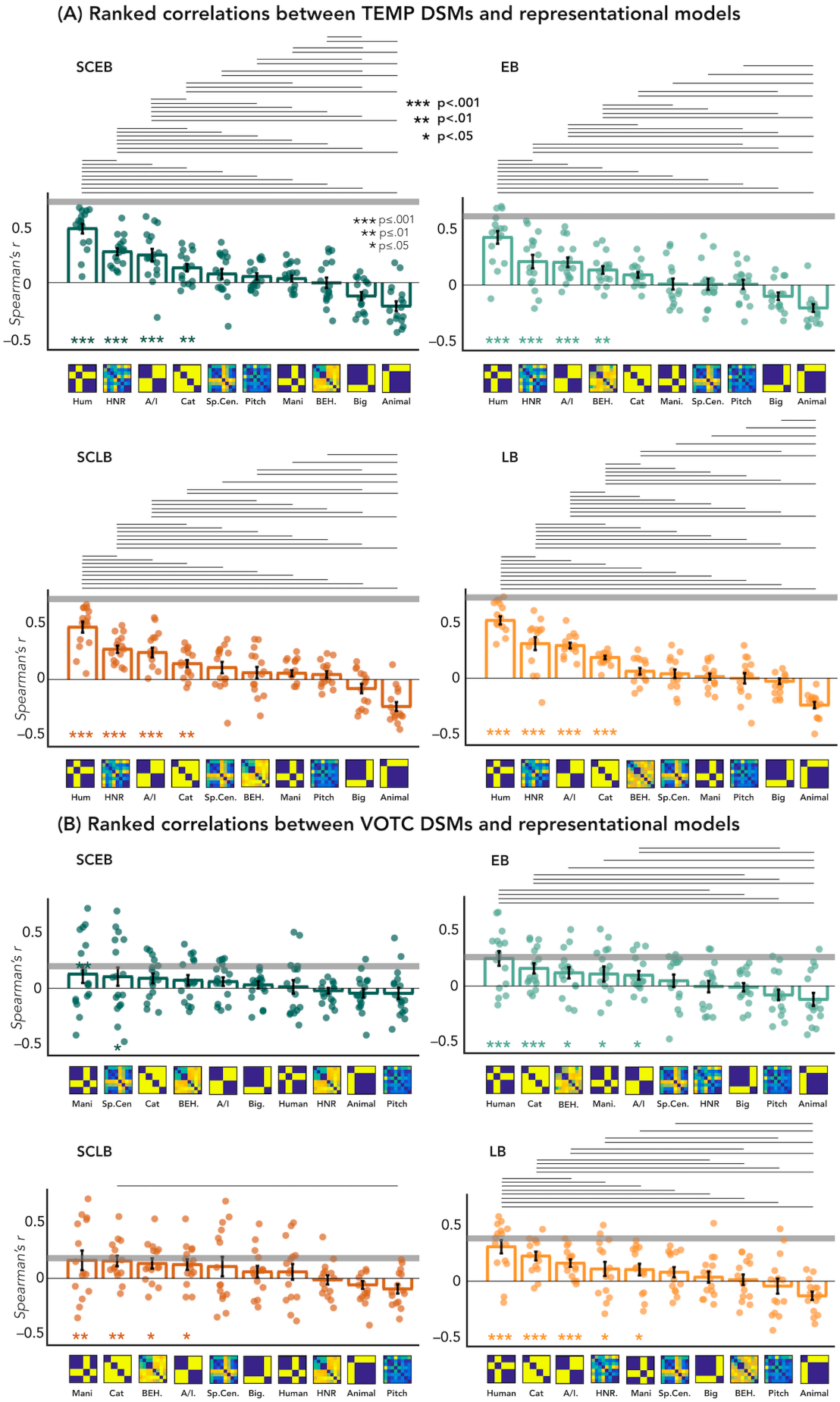
(A) Ranked correlations between TEMP DSMs and representational models
SCEB
EB
SCLB
LB
*** p<.001
** p<.01
* p<.05
*** p≤.001
** p≤.01
* p≤.05
Spearman's r
0.5
0
−0.5
Hum HNR A/I Cat Sp.Cen. Pitch Mani BEH. Big Animal
Hum HNR A/I BEH. Cat Mani. Sp.Cen. Pitch Big Animal
Hum HNR A/I Cat Sp.Cen. BEH. Mani Pitch Big Animal
Hum HNR A/I Cat BEH. Sp.Cen. Mani Pitch Big Animal
(B) Ranked correlations between VOTC DSMs and representational models
SCEB
EB
SCLB
LB
Mani Sp.Cen Cat BEH. A/I Big. Human HNR Animal Pitch
Human Cat BEH. Mani. A/I Sp.Cen. HNR Big Pitch Animal
Mani Cat BEH. A/I. Sp.Cen. Big. Human HNR Animal Pitch
Human Cat A/I. HNR. Mani Sp.Cen. Big BEH. Pitch Animal

Fig. 4. RSA-Correlation with representational models (A) Correlation between TEMP DSM of each group and the 10 representational models. (B) Correlation between VOTC DSM of each group and the 10 representational models. Bars show mean Spearman's correlations across participants, error bars show standard error and each dot represent one participant. Horizontal grey lines show the lower bound of the noise ceiling. An asterisk below the bar indicate that correlations with that model were significantly higher than zero. Correlations with individual models are sorted from highest to lowest. Horizontal lines above bars show significant differences between the correlations of the two end points (FDR corrected for multiple comparisons).

In fig. 4A we reported the ranked correlation between the temporal DSM in each group and each of the ten representational models (Animate-Inanimate, 4 categories, Behavioral, Human, Animal, Manipulable, Big & Place, HNR, Pitch, Spectral Centroid). See also figure 4 – supplemental fig2 to visualize the complete set of models and the correlation between them. The r values and the p values for each model and group are reported in table 7.

MODELS	GROUPS							
	SCEB		EB		SCLB		LB	
	r	*p*	*r*	*p*	*r*	*p*	*r*	*p*
Categorical	**.13**	.0007	.09	NS	**.14**	.0006	**.19**	.0005
Ani/Inani	**.25**	.0003	**.21**	.0007	**.24**	.0003	**.29**	.0003
Behav.	–.002	NS	**.14**	.003	.06	NS	.06	NS
Human	**.48**	.0003	**.44**	.0005	**.47**	.0003	**.52**	.0003
Animal	– .21	NS	– .21	NS	–.24	NS	–.24	NS
Manipulable	.04	NS	.01	NS	.06	NS	.01	NS
Big	–.12	NS	–.10	NS	–.08	NS	–.03	NS
HNR	**.28**	.0003	**.22**	.0005	**.27**	.0003	**.31**	.0003
Pitch	.05	NS	.007	NS	.04	NS	–.01	NS
Spect.Cent.	.08	NS	.007	NS	**.11**	.03	.04	NS

Table 7. R and p (FDR corrected for 10 comparisons) values from RSA correlation between Temporal DSM & external models

We also compared the correlations across all pairs of models within each ROI and group. For these pairwise comparisons, we used two-sided Wilcoxon signed-rank test and

only significant FDR corrected values (for 45 comparisons) are reported in Fig. 4 (Tsantani et al., 2020).

For the temporal ROIs, the human model was the winning model in each group (SCEB: r=0.48, p=0.0003; EB: r=0.44, p=0.0005; SCLB: r=0.47, p=0.0003; LB: r=0.52, p=0.0003), explaining the functional profile of the temporal regions more than all the others (see Fig. 4A).

In fig. 4B we reported the ranked correlation between the VOTC DSM in each group and each of the same ten representational models. The r values and the p values for each model and group are reported in table 8.

MODELS	GROUPS							
	SCEB		EB		SCLB		LB	
	r	*p*	*r*	*p*	*r*	*p*	*r*	*p*
Categorical	.09	NS	**.16**	.003	**.16**	.004	**.23**	.0005
Ani/Inani	.06	NS	**.10**	.05	**.12**	.02	**.17**	.001
Behav.	.07	NS	**.12**	.03	**.13**	.02	.01	NS
Human	.01	NS	**.25**	.001	.06	NS	**.32**	.0005
Animal	–.04	NS	–.12	NS	–.06	NS	–.13	NS
Manipulable	**.13**	.02	**.11**	.04	**.16**	.002	**.11**	.03
Big	.03	NS	–.01	NS	.06	NS	.04	NS
HNR	–.02	NS	–.01	NS	–.01	NS	**.11**	.02
Pitch	–.05	NS	–.08	NS	–.09	NS	–.04	NS
Spect.Cent.	**.10**	.03	.05	NS	.10	NS	.08	NS

Table 8. R and p values (FDR corrected for 10 comparisons) from RSA correlation between VOTC DSM & external models.

Similar to the temporal cortex of all groups, the human model showed the highest correlation with the DSM of VOTC only in the 2 groups of blind (EB: r=0.25, p=0.001; LB: r=0.32, p=0.0005), suggesting a possible explanation for the enhanced similarity between the TEMP DSMs and the VOTC DSMS of blind subjects (compared to sighted controls).

Since the human model is the one that explains most of the variance of our data in the temporal ROI of each group and in the VOTC of both blind groups, we run further

analyses for this model. That is, we directly investigated whether there was a statistical difference between groups in the correlation with the human model, both in VOTC and in temporal ROIs.

RSA results with the human model for the EB / SCEB groups are represented in figure 4-supplemental fig. 1 (left panel). The permutation test revealed a significantly higher correlation in EB compared to the SCEB (p=0.007). In the temporal ROI, instead, the correlation was not significantly different between SCEB and EB (p=0.26). Finally, the interaction 2 Groups X 2 ROIs (run using ART) revealed a significant effect of interaction group by region (p=0.0003).

RSA results with the human model for the LB / SCLB groups are represented in figure 4-supplemental fig. 1 (central panel). The permutation test revealed a significant difference between groups in the VOTC (p=0.005), while in the temporal ROI there was not a significant difference between LB and SCLB (p=0.23). The interaction 2 Groups X 2 ROIs (run using ART) revealed a significant interaction between group and region (p=0.000003).

Finally, we directly compared the correlation from the early and the late blind subjects, after a normalization of the data for each blind group based on its own sighted control group (Fig. 3B, right panel). The permutation test did not reveal any difference between the two groups neither in VOTC (p=0.5) nor in the temporal ROI (p=0.11).

Discussion (1500 w. max)

We investigated the link between cross-modal and intra-modal plasticity in early and late blind people during the processing of sounds from different categories. Compared to our previous paper on which we build on (Mattioni et al., 2020), the present study shed new lights on two fundamental issues: 1) How does the reorganization of occipital regions in EB impacts on the response profile of temporal regions typically coding for sounds, and 2) how does the age of blindness onset impacts on large-scale brain (re)organization. Both these issues will be discussed in succession in the following discussion. Overall our study goes beyond the comparison of activity level between groups by providing a comprehensive multi-voxel exploration of how blindness at different age of acquisition induces large-scale reorganization of the representation of sound categories in the brain.

We observed enhanced decoding accuracies in EB, when compared to SCEB, in the VOTC that is concomitant to reduced decoding accuracy in the temporal cortex (see figure 1B). From these results, we hypothesize that early visual deprivation triggers a relocation of auditory computation, typically carried out in the temporal cortex, toward the occipital cortex. Few studies relying on MVPA techniques recently reported similar results (Dormal et al., 2016, Jiang et al., 2016, Hurk et al., 2017). That is, an increased decodability of auditory stimuli in the occipital cortex and a decreased decodability of the auditory stimuli in the temporal regions of EB when compared to sighted controls. However, these studies did not deepen these initial results and did not focus on the link between intramodal and crossmodal reorganizations in early blind individuals.

Why would visual deprivation create such a redistribution of computational load between brain cortices? If we take a wider perspective, this phenomenon might be linked

to the homeostatic plasticity mechanisms, extensively described at the synaptic level (Keck et al., 2017; Turrigiano, 2012; Whitt, Petrus, & Lee, 2013). "Homeostatic plasticity" refers to the changes that allow neurons to adjust their activity and compensate for long periods of increased or decreased input activity. These stabilizing mechanisms are likely necessary to keep Hebbian changes to the system under control, and to avoid that the activity becomes extreme, either too high or too low (Keck et al., 2017). They, indeed, allow for the adjustment of overall neuronal activity while preserving the relative strength of individual synapses, and therefore they are crucial to maintain physiological functions in situations of chronic alterations in neuronal drive, such as the loss of a sensory modality (Whitt et al., 2013). Our results could, therefore, be explained by the homeostatic plasticity, representing the effort of the sensory cortices to adequately adapt to prolonged periods of visual deprivation.

Actually, such an imbalance mechanism has been reported by few studies also on deaf individuals (Bottari et al., 2014; Cardin et al., 2016; Sandmann et al., 2012) suggesting that, in the case of early auditory deprivation, additional visual computation performed within temporal areas decreases the perceptual load in occipital regions (Bottari et al., 2014). These results, therefore, suggest that the reallocation of the computational load from the regions coding for the spare senses to the reorganized cortex is not specific to visually deprived individuals but might be a general principle followed also by other kinds of sensory deprivation, as suggested by the homeostatic plasticity hypothesis.

Would this redistribution of computational load across temporal and occipital regions predict a representation of auditory category in VOTC that is more similar to the representation of the same auditory categories in the temporal regions in EB when

compared to SC? Our results suggest that this is indeed the case. With a set of within and between-subject analyses (Fig. 3) we showed an enhanced correlation between the functional profile of VOTC and the temporal region in EB subjects compared to SCEB. This result is supported by the hierarchical clustering analysis (Fig. 3C) showing that the VOTC of EB clusters together with the temporal regions of both EB and SCEB, instead of clustering with the VOTC of SCEB. This is a clear evidence that the way VOTC represents the auditory categories in EB is more similar to the way used by the temporal regions in both EB and SCEB subjects than to the way used by VOTC in sighted. Our results of a more similar neural representation of the stimuli between temporal and occipital regions in EB compared to SCEB is in line with previous studies showing an enhanced functional connectivity between occipital and temporal regions during sound processing in EB (Collignon et al., 2013; Dormal et al., 2016; Klinge, Eippert, Röder, & Büchel, 2010).

These findings suggest that the functional interconnection between the occipital and temporal regions is strengthen following early visual deprivation, allowing a flowing of information with an effective redistribution of the computational load between these two cortices.

How does blindness onset impact on this large-scale brain reorganization? Overall, we observed that the expression of brain reorganization in LB is somehow similar, but slightly less salient, to the one observed in EB. Similar to what we observed in EB (Mattioni et al., 2020), the topographical categorical map of VOTC in LB shows an important degree of similarity with the map of VOTC in sighted subjects for visual stimuli. The amount of this similarity did not differ from the one of EB and is significantly enhanced compared to the similarity between the maps of sighted in vision and sighted in audition. We also observed

that the decoding of auditory categories in VOTC is enhanced in LB when compared to SCLB, similar to the results of EB.

These evidences suggest that the reorganization of VOTC following blindness is not qualitatively affected by the onset at which visual deprivation occurs. These important results are in contrast with previous works reporting an absence of functionally selective recruitment of occipital regions in LB individuals (Marina Bedny et al., 2012; Cohen et al., 1999; Collignon et al., 2013; Kanjlia et al., 2019; Pant, Kanjlia, & Bedny, 2020). Our results are however in line with recent studies showing a categorical organization of lateral and ventral OTC that is already partially independent from vision in sighted (Mattioni et al., 2020; Peelen et al., 2013). Similar to what was observed in EB (Mattioni et al., 2020), we observed that visual deprivation occurring late in life follows organizational principle that are also rooted in the sighted's brain. We therefore suggest that early and late visual deprivation triggers an extension of the partially non-visual categorical organization of VOTC that is also seen in the sighted.

The second main aim of this study was to assess how blindness onset impacts the encoding of auditory categories across occipital and temporal regions. Similar to what was observed in EB, we observed that, when compared to SCLB, LB show enhanced representation of sound categories in VOTC while the temporal cortex shows lower decoding in LB (supported by a significant interaction group x region; see Fig. 1B). It is however important to note that when both regions are treated in isolation, decoding accuracies in LB were not statistically different from those of SCLB. This suggests that even if brain reorganizations in LB show qualitative similarities to those observed in EB, the expression of this plasticity might be quantitatively less robust when visual deprivation

occurs late in life (Marina Bedny & Saxe, 2012; Büchel, Price, Frackowiak, & Friston, 1998; Cohen et al., 1999; Collignon et al., 2013).

Similar to EB, we also found that the representation of auditory categories in VOTC was more similar to the one of temporal regions in LB when compared to the SCLB. The hierarchical clustering analysis highlights this result showing that also in the case of LB (as we saw above for the EB) the way VOTC represents the auditory categories is more similar to the way used by the temporal regions in both LB and SCLB subjects than to the way used by VOTC in sighted (see fig 3C, right panel).

When we directly compared the EB and LB data (both for the classification and for the correlation results), after normalizing them based on their own matched SC groups, we did not find any statistical difference between the two groups (see fig1B right panel and fig. 3A right panel). This suggests that brain reorganization expresses similarly in the two groups, revealing an analogous reorganizational profile in EB and LB with an extension of non-visual functions in their occipital cortex and a related relocation of the auditory processing that may reduce the computational load of the temporal regions.

What is the representation that makes the occipital and temporal functional profiles more similar in early and late blind groups when compared to sighted individuals? When compared to vision, little is known about how auditory categorization in implemented in the brain. Previous studies reported the presence of clusters of voxels within the superior temporal regions (Giordano, McAdams, Zatorre, Kriegeskorte, & Belin, 2013; Peelle, Johnsrude, & Davis, 2010), showing a preference for one specific category compared to others, such as human voices (Belin, Fecteau, & Bédard, 2004), instrumental sounds (Leaver & Rauschecker, 2010)or the sounds of objects (Dormal, Pelland, Rezk, & Yakobov, 2017; Lewis, Talkington, Puce, Engel, & Frum, 2011). However, most previous studies primarily focused on a relatively small number of categories. Therefore, the investigation for a more general dimension accounting for the categorical representation in the temporal cortex was

still missing. In the present study, we tried to fill this gap by looking at which model, among several types based on different categorical and acoustic dimensions (such as animacy, behavioral similarity judgment, categorical clustering, harmonicity, pitch, etc.), would better account for the representation of the auditory categories in the VOTC and temporal regions in both sighted and blind. In the temporal cortex, we found that in every group the best model was a "human" model, in which human stimuli were considered similar between themselves and different from all other animate and inanimate stimuli. This result is reminiscent of a recent MEG study reporting such a "human-centric' representation for visual stimuli in healthy subjects, providing evidence for a humanness dimension of visual objects represented in the human brain (Contini, Goddard, Grootswagers, Williams, & Carlson, 2019). Interestingly, we also found that the human model was significantly correlated with the representation of the auditory categories in VOTC of both our blind groups but not of the sighted controls. In addition, when compared to the other models, the human model was among the ones that better accounted for the representation of the auditory categories in VOTC of EB and LB, but not of the matched SC groups. This shared "human-centric" representation in both the temporal and occipital cortices of blind individuals therefore explains what drives the increased similarity between these two regions in visually deprived individuals.

To summarize, we discovered that in early blind, and to some extent in late blind people, the enhanced coding of sound categories in occipital regions is coupled with lower coding in the temporal regions compared to sighted people. Moreover, we observed a representation of auditory categories in VOTC more similar to the representation of the same auditory categories in the temporal regions in both early and late blind individuals when compared to their sighted controls. These findings suggest an interplay between the reorganization of occipital and temporal regions following visual deprivation, with a modulation of this process according to the onset of blindness. Crucially, the functional relevance of this reorganization is preserved also in case of late onset of blindness.

Figure's legend

Fig. 1. Experimental design and MVP-classification results using ROIs. (A) Categories of stimuli, design of the fMRI experiment and Regions of Interest (ROIs). (B) MVP-classification results. Left panel: results from the EB/SCEB groups;

central panel: results from the LB/SCLB groups; right panel: data from EB and LB are directly compared after normalizing them based on their own matched group.

Fig. 1. Supplemental fig. 1. MVP-classification results using searchlight.

Fig. 2. Topographical selectivity maps. Averaged untresholded topographical selectivity maps for the early blind (EB, bottom left), and their matched sighted controls (SCEB, top left), the late blind (LB, bottom right) and their matched sighted controls (SCLB, top left). In the center we also reported the map from an additional group of sighted that perform the visual version of the experiment. These maps visualize the functional topography of VOTC and TEMP to the main four categories in each group. These group maps are created for visualization purpose only since statistics are run from single subject maps (see methods). To obtain those group maps, we first averaged the β-values among participants of the same group in each voxel inside the VOTC and inside the TEMP mask for each of our 4 main conditions (animals, humans, manipulable objects and places) separately and we then assigned to each voxel the condition producing the highest β-value.

Fig. 3. Correlation between VOTC and TEMP DSMs. (A) Correlation between VOTC and TEMPORAL DSMs within each subjects. Each dot represents the Spearman's correlation of each subject between its own VOTC and TEMP DSMs. Left panel: results from the EB/SCEB groups; central panel: results from the LB/SCLB groups; right panel: data from EB and LB are directly compared after normalizing them based on their own matched group. (B) Correlation between VOTC and TEMPORAL DSMs between subjects and groups. Each matrix represents the group averaged DSM of each ROI (top row: VOTC, bottom row: TEMP). The arrows between each pair of matrices represents the averaged Spearman's correlation between the 2 DSMs. Thicker the arrow, higher the correlation value. In the box on the left side (EB/SCEB) and on the right side (LB/SCLB) we report the statistical differences in the strength of similarity between the most important pair of matrices (color-coded in red, light-blue and purple).

Fig. 3 Supplemental fig 1. Correlation between VOTC and TEMP DSMs between subject and groups using bar plots. The correlations valued form the figure 3B are represented here using bar graph visualization. Each dot represents a subject. Left panel: data from EB/SCEB; right panel: data from LB/SCLB.

Fig. 4. RSA-Correlation with representational models (A) Correlation between TEMP DSM of each group and the 10 representational models. (B) Correlation between VOTC DSM of each group and the 10 representational models. Bars show mean Spearman's correlations across participants, error bars show standard error and each dot represent one participant. Horizontal grey lines show the lower bound of the noise ceiling. An asterisk below the bar indicate that correlations with that model were significantly higher than zero. Correlations with individual models are sorted from highest to lowest. Horizontal lines above bars show significant differences between the correlations of the two end points (FDR corrected for multiple comparisons).

Fig. 4 Supplemental fig 1. Representational models. (A) Representation of all candidate models. There are for different behavioral models, one for each group. (B) Matrix including the linear correlations between each pair of models. Yellow indicates high correlations, blue indicated low correlation.

Fig. 4 Supplemental fig 2. RSA results with the Human model: between group's comparisons. Spearman's correlation between the DSMs in the 2 ROIs (VOTC and TEMP) with the human model. Left panel: results from the EB/SCEB groups; central panel: results from the LB/SCLB groups; right panel: data from EB and LB are directly compared after normalizing them based on their own matched control group.

References

Ackeren, M. J. Van, Barbero, F. M., Mattioni, S., Bottini, R., Van Ackeren, M. J., Barbero, F. M., … Collignon, O. (2018). Neuronal populations in the occipital cortex of the blind synchronize to the temporal dynamics of speech. *ELife*, *7*, 1–20. https://doi.org/10.7554/eLife.31640

Amedi, A., Jacobson, G., Hendler, T., Malach, R., & Zohary, E. (2002). Convergence of visual and tactile shape processing in the human lateral occipital complex. *Cerebral Cortex (New York, N.Y. : 1991)*, *12*(11), 1202–1212. Retrieved from http://www.ncbi.nlm.nih.gov/pubmed/12379608

Amedi, A., Raz, N., Azulay, H., Malach, R., & Zohary, E. (2010). Cortical activity during tactile exploration of objects in blind and sighted humans. *Restorative Neurology and Neuroscience*, *28*(2), 143–156. https://doi.org/10.3233/RNN-2010-0503

Amedi, A., Raz, N., Pianka, P., Malach, R., & Zohary, E. (2003). Early "visual" cortex activation correlates with superior verbal memory performance in the blind. *Nature Neuroscience*, *6*(7), 758–766. https://doi.org/10.1038/nn1072

Ashburner, J. (2007). A fast diffeomorphic image registration algorithm. *NeuroImage*, *38*(1), 95–113. https://doi.org/10.1016/j.neuroimage.2007.07.007

Bedny, M., Richardson, H., & Saxe, R. (2015). "Visual" Cortex Responds to Spoken

Language in Blind Children. *Journal of Neuroscience*, *35*(33), 11674–11681. https://doi.org/10.1523/JNEUROSCI.0634-15.2015

Bedny, Marina, Pascual-Leone, A., Dodell-Feder, D., Fedorenko, E., & Saxe, R. (2011). Language processing in the occipital cortex of congenitally blind adults. *Proceedings of the National Academy of Sciences of the United States of America*, *108*(11), 4429–4434. https://doi.org/10.1073/pnas.1014818108

Bedny, Marina, Pascual-Leone, A., Dravida, S., & Saxe, R. (2012). A sensitive period for language in the visual cortex: distinct patterns of plasticity in congenitally versus late blind adults. *Brain and Language*, *122*(3), 162–170. https://doi.org/10.1016/j.bandl.2011.10.005

Bedny, Marina, & Saxe, R. (2012). Insights into the origins of knowledge from the cognitive neuroscience of blindness. *Cognitive Neuropsychology*, *29*(December), 56–84. https://doi.org/10.1080/02643294.2012.713342

Belin, P., Fecteau, S., & Bédard, C. (2004). Thinking the voice: Neural correlates of voice perception. *Trends in Cognitive Sciences*. https://doi.org/10.1016/j.tics.2004.01.008

Benjamini, Y., & Hochberg, Y. (1995). Benjamini-1995.pdf. *Journal of the Royal Statistical Society B*.

Berlot, E., Popp, N. J., & Diedrichsen, J. (2020). fMRI signatures of motor sequence learning: A critical re-evaluation. *BioRxiv*, 2020.01.08.899229. https://doi.org/10.1101/2020.01.08.899229

Bottari, D., Heimler, B., Caclin, A., Dalmolin, A., Giard, M., & Pavani, F. (2014). NeuroImage Visual change detection recruits auditory cortices in early deafness, *94*, 172–184.

Büchel, C., Price, C., Frackowiak, R. S., & Friston, K. (1998). Different activation patterns in

the visual cortex of late and congenitally blind subjects. *Brain : A Journal of Neurology*, *121 (Pt 3*, 409–419. Retrieved from http://www.ncbi.nlm.nih.gov/pubmed/9549517

Burton, H., Snyder, A. Z., Conturo, T. E., Akbudak, E., Ollinger, J. M., & Raichle, M. E. (2002). Adaptive Changes in Early and Late Blind: A fMRI Study of Braille Reading. *Journal of Neurophysiology*, *87*(1), 589–607. https://doi.org/10.1152/jn.00129.2002

Cardin, V., Smittenaar, R. C., Orfanidou, E., Rönnberg, J., Capek, C. M., Rudner, M., & Woll, B. (2016). Differential activity in Heschl's gyrus between deaf and hearing individuals is due to auditory deprivation rather than language modality. *NeuroImage*, *124*, 96–106. https://doi.org/10.1016/j.neuroimage.2015.08.073

Cohen, L. G., Weeks, R. A., Sadato, N., Celnik, P., Ishii, K., & Hallett, M. (1999). Period of susceptibility for cross-modal plasticity in the blind. *Annals of Neurology*, *45*(4), 451–460. https://doi.org/10.1002/1531-8249(199904)45:4<451::AID-ANA6>3.0.CO;2-B

Collignon, O., Dormal, G., Albouy, G., Vandewalle, G., Voss, P., Phillips, C., & Lepore, F. (2013). Impact of blindness onset on the functional organization and the connectivity of the occipital cortex. *Brain*, *136*(9), 2769–2783. https://doi.org/10.1093/brain/awt176

Collignon, O., Vandewalle, G., Voss, P., Albouy, G., Charbonneau, G., Lassonde, M., & Lepore, F. (2011). Functional specialization for auditory-spatial processing in the occipital cortex of congenitally blind humans. *Proceedings of the National Academy of Sciences of the United States of America*, *108*(11), 4435–4440. https://doi.org/10.1073/pnas.1013928108

Conover, W. J., & Iman, R. L. (1981). Rank transformations as a bridge between parametric and nonparametric statistics. *American Statistician*. https://doi.org/10.1080/00031305.1981.10479327

Contini, E. W., Goddard, E., Grootswagers, T., Williams, M., & Carlson, T. (2019). A humanness dimension to visual object coding in the brain. *BioRxiv*, (May), 648998. https://doi.org/10.1101/648998

De Martino, F., Valente, G., Staeren, N., Ashburner, J., Goebel, R., & Formisano, E. (2008). Combining multivariate voxel selection and support vector machines for mapping and classification of fMRI spatial patterns. *NeuroImage*, *43*(1), 44–58. https://doi.org/10.1016/j.neuroimage.2008.06.037

Desikan, R. S., Ségonne, F., Fischl, B., Quinn, B. T., Dickerson, B. C., Blacker, D., … Killiany, R. J. (2006). An automated labeling system for subdividing the human cerebral cortex on MRI scans into gyral based regions of interest. *NeuroImage*, *31*(3), 968–980. https://doi.org/10.1016/j.neuroimage.2006.01.021

Dormal, G., & Collignon, O. (2011). Functional selectivity in sensory-deprived cortices. *Journal of Neurophysiology*, *105*(6), 2627–2630. https://doi.org/10.1152/jn.00109.2011

Dormal, G., Pelland, M., Rezk, M., & Yakobov, E. (2017). Functional Preference for Object Sounds but Not for Voices in the Occipitotemporal Cortex of Early Blind Individuals, 1–21. https://doi.org/10.1162/jocn

Dormal, G., Rezk, M., Yakobov, E., Lepore, F., & Collignon, O. (2016). NeuroImage Auditory motion in the sighted and blind : Early visual deprivation triggers a large-scale imbalance between auditory and " visual " brain regions. *NeuroImage*, *134*, 630–644. https://doi.org/10.1016/j.neuroimage.2016.04.027

Elbert, T., Sterr, A., Rockstroh, B., Pantev, C., & Mu, M. M. (2002). Expansion of the Tonotopic Area in the Auditory Cortex of the Blind, *22*(22), 9941–9944.

Etzel, J. A., Zacks, J. M., & Braver, T. S. (2013). Searchlight analysis: Promise, pitfalls, and potential. *NeuroImage*. https://doi.org/10.1016/j.neuroimage.2013.03.041

Evans, S., Price, C. J., Diedrichsen, J., Gutierrez-Sigut, E., & MacSweeney, M. (2019). Sign and Speech Share Partially Overlapping Conceptual Representations. *Current Biology*, *29*(21), 3739-3747.e5. https://doi.org/10.1016/j.cub.2019.08.075

Giordano, B. L., McAdams, S., Zatorre, R. J., Kriegeskorte, N., & Belin, P. (2013). Abstract encoding of auditory objects in cortical activity patterns. *Cerebral Cortex (New York, N.Y. : 1991)*, *23*(9), 2025–2037. https://doi.org/10.1093/cercor/bhs162

Gougoux, F., Belin, P., Voss, P., Lepore, F., Lassonde, M., & Zatorre, R. J. (2009). Voice perception in blind persons: a functional magnetic resonance imaging study. *Neuropsychologia*, *47*(13), 2967–2974. https://doi.org/10.1016/j.neuropsychologia.2009.06.027

Hurk, J. Van Den, Baelen, M. Van, Op, H. P., & Beeck, D. (2017). Development of visual category selectivity in ventral visual cortex does not require visual experience, 1–10. https://doi.org/10.1073/pnas.1612862114

Jiang, F., Stecker, G. C., Boynton, G. M., & Fine, I. (2016). Early Blindness Results in Developmental Plasticity for Auditory Motion Processing within Auditory and Occipital Cortex, *10*(July). https://doi.org/10.3389/fnhum.2016.00324

Jiang, J., Zhu, W., Shi, F., Liu, Y., Li, J., Qin, W., … Jiang, T. (2009). Thick Visual Cortex in the Early Blind. *Journal of Neuroscience*, *29*(7), 2205–2211. https://doi.org/10.1523/JNEUROSCI.5451-08.2009

Kanjlia, S., Pant, R., & Bedny, M. (2019). Sensitive Period for Cognitive Repurposing of Human Visual Cortex. *Cerebral Cortex (New York, N.Y. : 1991)*, *29*(9), 3993–4005.

https://doi.org/10.1093/cercor/bhy280

Keck, T., Toyoizumi, T., Chen, L., Doiron, B., Feldman, D. E., Fox, K., … van Rossum, M. C. (2017). Integrating Hebbian and homeostatic plasticity: The current state of the field and future research directions. *Philosophical Transactions of the Royal Society B: Biological Sciences*, *372*(1715). https://doi.org/10.1098/rstb.2016.0158

Klinge, C., Eippert, F., Röder, B., & Büchel, C. (2010). Corticocortical connections mediate primary visual cortex responses to auditory stimulation in the blind. *The Journal of Neuroscience : The Official Journal of the Society for Neuroscience*, *30*(38), 12798–12805. https://doi.org/10.1523/JNEUROSCI.2384-10.2010

Kriegeskorte, N., & Kievit, R. a. (2013). Representational geometry: integrating cognition, computation, and the brain. *Trends in Cognitive Sciences*, *17*(8), 401–412. https://doi.org/10.1016/j.tics.2013.06.007

Kriegeskorte, N., & Mur, M. (2012). Kriegeskorte.2012. *Frontiers in Psychology*.

Kriegeskorte, N., Mur, M., & Bandettini, P. (2008). Representational similarity analysis - connecting the branches of systems neuroscience. *Frontiers in Systems Neuroscience*, *2*(November), 4. https://doi.org/10.3389/neuro.06.004.2008

Kriegeskorte, N., Mur, M., Ruff, D. A., Kiani, R., Bodurka, J., Esteky, H., … Bandettini, P. A. (2008). Matching Categorical Object Representations in Inferior Temporal Cortex of Man and Monkey. *Neuron*, *60*(6), 1126–1141. https://doi.org/10.1016/j.neuron.2008.10.043

Leaver, A. M., & Rauschecker, J. P. (2010). Cortical representation of natural complex sounds: effects of acoustic features and auditory object category. *The Journal of Neuroscience : The Official Journal of the Society for Neuroscience*, *30*(22), 7604–

7612. https://doi.org/10.1523/JNEUROSCI.0296-10.2010

Lewis, J. W., Talkington, W. J., Puce, A., Engel, L. R., & Frum, C. (2011). Cortical networks representing object categories and high-level attributes of familiar real-world action sounds. *Journal of Cognitive Neuroscience*, *23*(8), 2079–2101. https://doi.org/10.1162/jocn.2010.21570

Leys, C., & Schumann, S. (2010). A nonparametric method to analyze interactions: The adjusted rank transform test. *Journal of Experimental Social Psychology*, *46*(4), 684–688. https://doi.org/10.1016/j.jesp.2010.02.007

Manjunath, N. K., Srinivas, R., Nirmala, K. S., Nagendra, H. R., Kumar, a, & Telles, S. (1998). Shorter latencies of components of middle latency auditory evoked potentials in congenitally blind compared to normal sighted subjects. *The International Journal of Neuroscience*. https://doi.org/10.3109/00207459809003339

Mattioni, S., Rezk, M., Battal, C., Bottini, R., Mendoza, K. E. C., Oosterhof, N. N., & Collignon, O. (2020). Categorical representation from sound and sight in the ventral occipito-temporal cortex of sighted and blind, 1–33.

Mitchell, T. M., & Wang, X. (2007). Learning to decode instantaneous cognitive states from brain images. *Proceedings of the Frontiers in the Convergence of Bioscience and Information Technologies, FBIT 2007*, 458–461. https://doi.org/10.1109/FBIT.2007.150

Naveen, K. V, Srinivas, R., Nirmala, K. S., Nagarathna, R., Nagendra, H. R., & Telles, S. (1998). Differences between congenitally blind and normally sighted subjects in the P1 component of middle latency auditory evoked potentials. *Perceptual and Motor Skills*. https://doi.org/10.2466/pms.1998.86.3c.1192

Norman, K. a, Polyn, S. M., Detre, G. J., & Haxby, J. V. (2006). Beyond mind-reading: multi-

voxel pattern analysis of fMRI data. *Trends in Cognitive Sciences*, *10*(9), 424–430. https://doi.org/10.1016/j.tics.2006.07.005

Oosterhof, N. N., Connolly, A. C., & Haxby, J. V. (2016). CoSMoMVPA: Multi-Modal Multivariate Pattern Analysis of Neuroimaging Data in Matlab/GNU Octave. *Frontiers in Neuroinformatics*, *10*(July), 1–27. https://doi.org/10.3389/fninf.2016.00027

Pan, W. J., Wu, G., Li, C. X., Lin, F., Sun, J., & Lei, H. (2007). Progressive atrophy in the optic pathway and visual cortex of early blind Chinese adults: A voxel-based morphometry magnetic resonance imaging study. *NeuroImage*, *37*(1), 212–220. https://doi.org/10.1016/j.neuroimage.2007.05.014

Pant, R., Kanjlia, S., & Bedny, M. (2020). A sensitive period in the neural phenotype of language in blind individuals. *Developmental Cognitive Neuroscience*, *41*, 100744. https://doi.org/10.1016/j.dcn.2019.100744

Park, H., Doo, J., Yeop, E., Park, B., Oh, M., Lee, S., & Kim, J. (2009). NeuroImage Morphological alterations in the congenital blind based on the analysis of cortical thickness and surface area ☆. *NeuroImage*, *47*(1), 98–106. https://doi.org/10.1016/j.neuroimage.2009.03.076

Pascual-leone, A., & Torres, F. (1993). Plasticity of the sensorimotor cortex representation of the reading finger in Braille readers.

Peelen, M., Bracci, S., Lu, X., He, C., Caramazza, A., & Bi, Y. (2013). Tool selectivity in left occipitotemporal cortex develops without vision, 1–10. https://doi.org/10.1162/jocn

Peelle, J. E., Johnsrude, I. S., & Davis, M. H. (2010). Hierarchical processing for speech in human auditory cortex and beyond. *Frontiers in Human Neuroscience*, *4*, 51. https://doi.org/Artn 51\rDoi 10.3389/Fnhum.2010.00051

Pietrini, P., Furey, M. L., Ricciardi, E., Gobbini, M. I., Wu, W.-H. C., Cohen, L., … Haxby, J. V. (2004). Beyond sensory images: Object-based representation in the human ventral pathway. *Proceedings of the National Academy of Sciences of the United States of America*, *101*(15), 5658–5663. https://doi.org/10.1073/pnas.0400707101

Rauschecker, J. P. (2002). Cortical map plasticity in animals and humans. *Progress in Brain Research*, *138*, 73–88. https://doi.org/10.1016/S0079-6123(02)38072-5

Ricciardi, E., Bonino, D., Pellegrini, S., & Pietrini, P. (2014). Mind the blind brain to understand the sighted one! Is there a supramodal cortical functional architecture? *Neuroscience and Biobehavioral Reviews*, *41*, 64–77. https://doi.org/10.1016/j.neubiorev.2013.10.006

Ricciardi, E., Bonino, D., Sani, L., Vecchi, T., Guazzelli, M., Haxby, J. V, … Pietrini, P. (2009). Do we really need vision? How blind people "see" the actions of others. *The Journal of Neuroscience : The Official Journal of the Society for Neuroscience*, *29*(31), 9719–9724. https://doi.org/10.1523/JNEUROSCI.0274-09.2009

Ricciardi, E., & Pietrini, P. (2011). New light from the dark: What blindness can teach us about brain function. *Current Opinion in Neurology*, *24*(4), 357–363. https://doi.org/10.1097/WCO.0b013e328348bdbf

Röder, B., Stock, O., Bien, S., Neville, H., & Rösler, F. (2002). Speech processing activates visual cortex in congenitally blind humans. *European Journal of Neuroscience*, *16*(5), 930–936. https://doi.org/10.1046/j.1460-9568.2002.02147.x

Sadato, N., Pascual-Leone, A., Grafman, J., Ibanez, V., Deiber, M. P., Dold, G., & Hallett, M. (1996). Pictures and Page Numbers Image, Text and Formal Structure in the Visual Book and the Artist's Book. *Nature*. Retrieved from

http://www.christofflab.ca/pdfs/2009/01/sadato-et-al-1996.pdf

Sandmann, P., Dillier, N., Eichele, T., Meyer, M., Kegel, A., Pascual-Marqui, R. D., … Debener, S. (2012). Visual activation of auditory cortex reflects maladaptive plasticity in cochlear implant users. *Brain*, *135*(2), 555–568. https://doi.org/10.1093/brain/awr329

Stelzer, J., Chen, Y., & Turner, R. (2013). Statistical inference and multiple testing correction in classification-based multi-voxel pattern analysis (MVPA): Random permutations and cluster size control. *NeuroImage*, *65*, 69–82. https://doi.org/10.1016/j.neuroimage.2012.09.063

Stevens, A. A., & Weaver, K. E. (2009). Functional characteristics of auditory cortex in the blind, *196*, 134–138. https://doi.org/10.1016/j.bbr.2008.07.041

Striem-Amit, E., Cohen, L., Dehaene, S., & Amedi, A. (2012). Reading with Sounds: Sensory Substitution Selectively Activates the Visual Word Form Area in the Blind. *Neuron*, *76*(3), 640–652. https://doi.org/10.1016/j.neuron.2012.08.026

Striem-Amit, E., Dakwar, O., Reich, L., & Amedi, A. (2012). The large-scale organization of "visual" streams emerges without visual experience. *Cerebral Cortex (New York, N.Y. : 1991)*, *22*(7), 1698–1709. https://doi.org/10.1093/cercor/bhr253

Tsantani, M., Storrs, K., & Williams, A. L. (2020). FFA and OFA encode distinct types of face identity information, 1–23.

Turrigiano, G. (2012). Homeostatic synaptic plasticity: Local and global mechanisms for stabilizing neuronal function. *Cold Spring Harbor Perspectives in Biology*, *4*(1), 1–18. https://doi.org/10.1101/cshperspect.a005736

Wallmeier, L., Kish, D., Wiegrebe, L., & Flanagin, V. L. (2015). Aural localization of silent objects by active human biosonar : neural representations of virtual echo-acoustic

space, *41*(September 2014), 533–545. https://doi.org/10.1111/ejn.12843

Walther, A., Nili, H., Ejaz, N., Alink, A., Kriegeskorte, N., & Diedrichsen, J. (2016). Reliability of dissimilarity measures for multi-voxel pattern analysis. *NeuroImage*, *137*, 188–200. https://doi.org/10.1016/j.neuroimage.2015.12.012

Whitt, J. L., Petrus, E., & Lee, H. (2013). Author ' s personal copy Neuropharmacology Experience-dependent homeostatic synaptic plasticity in neocortex.

Zeng, H., & Constable, R. T. (2002). Image distortion correction in EPI: Comparison of field mapping with point spread function mapping. *Magnetic Resonance in Medicine*, *48*(1), 137–146. https://doi.org/10.1002/mrm.10200

Acknowledgement: This work was supported by a European Research Council starting grant (MADVIS grant #337573) attributed to OC and the Belgian Excellence of Science program (EOS Project No. 30991544) attributed to OC. MR is a research fellow and OC a research associate at the National Fund for Scientific Research of Belgium (FRS-FNRS). We are also extremely thankful to our blind participants and to the Unioni Ciechi of Trento, Mantova, Genova, Savona, Cuneo, Torino, Trieste and Milano and the blind Institute of Milano for helping with the recruitment.

Author contributions: SM and OC designed the research; SM, MR, CB and OC performed the research; SM, MR, CB, JV, and OC analyzed the data; SM and OC wrote the paper; MR, CB and JV gave feed-backs on a draft of the manuscript.